Robust Online Diagnosis of Inverter Open-circuit Switching Faults for Robotic Joints with BLDC Motors

Mohamed Y. Metwly, Landon Clark, Biyun Xie, JiangBiao He
Department of Electrical and Computer Engineering
University of Kentucky
Lexington, KY, USA
Email: mohamed.metwly@uky.edu

2024 IEEE Applied Power Electronics Conference and Exposition (APEC) | 979-8-3503-1664-3/24/$31.00 ©2024 IEEE | DOI: 10.1109/APEC48139.2024.10509158

***Abstract*—Online health monitoring of robotic joint motor drive systems is of paramount importance for robots utilized in remote, safety-critical, and hazardous environments. Joint motors and the associated power electronic drives are prone to hardware failures in harsh environments and may yield joint failures. Brushless DC (BLDC) motors and the related inverters have been considerably used in robotic arms; therefore, numerous inverter fault diagnostic strategies for BLDC motor drives have been proposed in recent literature to enhance the system's reliability and avoid downtime cost. In this paper, a robust fault diagnosis technique of semiconductor switches is proposed for BLDC motor drive systems in robotic applications based on the stator current signature analysis. The performance of the BLDC joint motors is investigated under inverter switches' open-circuit faults using finite element (FE) co-simulation tools. Besides the robust fault diagnosis capability, the proposed methodology is capable of identifying the faulty switch based on a knowledge table by considering several fault conditions. The robustness of the proposed technique has been verified through extensive simulations under numerous speed and load scenarios. Finally, theoretical findings are validated using the Kinova Gen3 robot arm to highlight the effect of joint faults on the robot's reachability of desired task locations.**

Keywords*—Joint motors, online fault diagnosis, inverter switches faults, collaborative robots, robustness analysis

I. Introduction

Due to their improved safety, flexibility, and productivity, robots have been utilized in numerous applications, e.g., space exploration [1], remediation of nuclear waste [2], surgical applications [3], human-robot interaction [4], and rescue missions [5]. Since more and more robots are used in harsh environmental conditions, e.g., high temperature and radiation, hardware failures of the joint motors and power electronic drives are likely to occur [6]. These failures may cause malfunction of the robotic arm. Thus, robot protection is of paramount importance to avoid economic loss and ensure the capability of robots to continuously operate when unforeseen failures and deterioration happen [7].

Brushed DC motors, Brushless DC (BLDC) motors, AC motors, DC linear actuators, stepper motors, and servo motors are among the commonly used electric motors in robotic applications [8]. A steeper, servo, and BLDC motors have been used in seven degrees-of-freedom (DOF) robotic manipulator [9], 7-DOF robotic arm [10], and applications in robotics [11], respectively. It is worth mentioning that stepper motors exhibit low cost and high starting torque. On the contrary, high torque ripple and low power density are the main demerits of stepper motors. Servo motors can also be utilized for robotic arms owing to their high efficiency and power density; however, their main disadvantages include complicated control and high overall cost. BLDC motors have shown promise in robotic applications. For instance, Fig. 1 depicts the Kinova Gen3 robotic arm which employs seven BLDC joint motors. Thus, BLDC motor drives are selected in this work [12]. BLDC motors offer high torque-producing capability and low maintenance costs. On the other hand, the high torque ripple constitutes the main drawback.

Several faults may happen in a BLDC motor drive, such as stator, rotor, or inverter semiconductor faults [13, 14]. Inverters play a major role in BLDC drive systems. Inverter open- and short-circuit faults represent 38% of failures in BLDC motor drive systems [15]. Therefore, robust diagnosis of inverters' open-circuit faults is crucial to minimize the downtime cost and potentially improve the reliability of robotic arms.

Various fault diagnosis methods have been presented in the literature for BLDC motor drives [16, 17]. Fault diagnostic techniques are categorized into model-based, signal analysis, and knowledge-based methods with further classification into time- and frequency-domain diagnosis. First, the model-based inverter switch fault diagnosis is achieved by comparing the actual and theoretical outputs of the model.

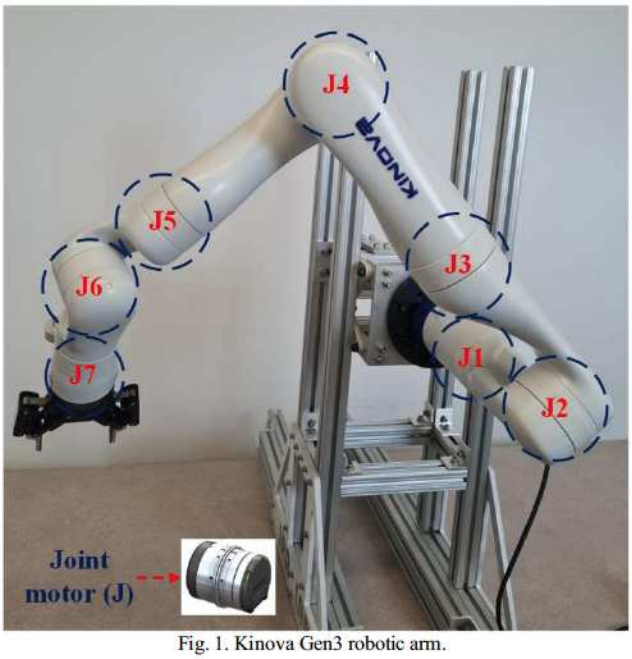

Fig. 1. Kinova Gen3 robotic arm.

This material is based upon work supported by the U.S. National Science Foundation (NSF) under Grant No. 2205292.

For example, an inverter open-circuit fault detection has been introduced for permanent magnet synchronous machine (PMSM) drives based on model predictive control (MPC) and cost function error. In this case, the estimated cost function is compared to the actual one, and the error is investigated to localize the fault [18]. Despite the fact that no additional hardware is entailed for model-based fault diagnostics, these techniques mainly depend on the accuracy of the model and its parameter estimation.

Furthermore, faults are detected by comparing measured features of the motor signals with the optimal condition when signal analysis methods are used. In [19], a simple diagnostic method for open-circuit faults in BLDC motor drives was introduced based on the current signature information. The proposed method requires no additional sensors to identify the fault conditions and the proposed algorithm can be embedded into the BLDC drive software without extra computational burden. Unlike the voltage signal analysis diagnosis techniques which are fast and require voltage acquisition circuitry, the fault diagnosis methods based on the current signature analysis are simple and low-cost [20]. Finally, the knowledge-based inverter fault detection methods for motor drives utilize fuzzy logic or neural networks exploiting the full knowledge of the system [16]. For instance, a fuzzy-based inverter fault diagnosis technique has been proposed for PMSM drive systems based on the motor current park's vector representation [21]. The proposed fault detection method is capable of detecting and localizing various inverter open-circuit faults, e.g., single, multiple, and intermittent faults. Some systems employ two distinct fault detection methods to make the best use of their merits [16].

Unlike conventional fault diagnosis techniques that lack robustness against speed and load variations, this paper presents a robust online fault diagnosis methodology for BLDC motor drives under inverter switch open-circuit faults. The proposed technique is based on discrete Fourier transform (DFT) analysis of the measured stator currents. The proposed fault detection method leverages the advantages of using the current signal analysis for fault detection and a knowledge-based table for fault identification. The effectiveness of the proposed diagnostic method is verified using finite element analysis (FEA) co-simulation tools. Specifically, the BLDC motor is optimally designed for robotic applications using the Ansys Electronics Desktop. The 2-level 3-phase inverter is built in Ansys Twin Builder, and the BLDC motor control is implemented in Simulink. Finally, simulations are conducted on the Kinova Gen3 robot arm to verify the proposed diagnostic technique using PyBullet software.

II. Proposed Fault Diagnosis Methodology

The architecture of the proposed BLDC motor drive system in Ansys Twin Builder is depicted in Fig. 2. The BLDC drive system consists of a three-phase 18-slot/10-pole BLDC motor powered by a 2-level 3-phase inverter through the phase resistance and leakage inductance and controlled by a BLDC current controller. The BLDC motor with fractional-slot winding is first designed based on the FEA and optimized based on the multi-objective genetic algorithm (MOGA), considering the average output torque, torque ripple, and core losses as the optimization objectives. The overall design optimization process has been performed using the Ansys Electronics Desktop. Table I reveals the motor design parameters. Basically, the BLDC motor is fed by a square-wave drive by exciting two phases at a time and gives a trapezoidal back EMF. In this case, the voltage source inverter and the BLDC current controller are implemented using Ansys Twin Builder and Simulink, respectively. The proposed fault diagnosis method utilizes the changes in the stator phase current as fault signatures. When the open-circuit fault of the switch occurs, the current waveform changes depending on where the faulty switch is located. In that case, current waveform patterns provide a straightforward method to identify the open-circuit fault.

Discrete Fourier Transform (DFT) spectral analysis of the BLDC motor phase currents is used to detect switches' open-circuit faults, as given by Eq. (1-3). Energy spectral density (ESD) for each phase is calculated at each time interval which is determined by the motor speed. The ESD values are compared at each time interval with the previous time interval to determine the ESD error of each phase. Accordingly, a fault is detected if the ESD errors of the stator phase currents exceed the 5% ESD error under the healthy case. The ESD error percentage is determined to avert the diagnosis of any short-term disturbance.

$$I(f) = \sum_{n=0}^{N-1} i_n \, e^{-2\pi i k n/N} \qquad 0 \le k \le N-1 \qquad (1)$$

$$S_m(f) = |I(f)|^2 \qquad (2)$$

$$error = S_m(f) - S_{m-1}(f) \qquad (3)$$

where $S_m(f)$ and $S_{m-1}(f)$ are the ESD after and before the fault, respectively, and $error$ is the ESD error.

The proposed fault diagnosis technique is designed to analyze the BLDC motor performance when the switches of the inverter fail. The BLDC motor drive is tested at the rated speed and load conditions, i.e., 1500 rpm rated speed and 1 Nm load torque. Under the switch S_1 open-circuit fault, the ESD values are measured before and after the switch fault for the three phases. The values of the measured ESD errors for the three phases are listed in Table II for the open-circuit faults of switches S_1 and S_4. It is clear that the maximum ESD error corresponds to phase A, i.e., the faulty phase. The same conclusion can be drawn under the S_4 open-circuit fault at which the maximum ESD error is related to phase A. Furthermore, simulation results have been carried out for the remaining switches of phase B and phase C. Owing to the symmetry of the BLDC motor, the ESD errors of phase A can be generalized for the remaining phases.

TABLE I. Design Parameters of the BLDC Motor

Power (W)	157
Rated speed (rpm)	1500
Rated torque (Nm)	1
DC link voltage (V)	48
Electric loading (A/mm)	12
Stator outer diameter (mm)	68.8
Stack length (mm)	62
Air gap length (mm)	0.5
Phase resistance (Ω)	0.1646

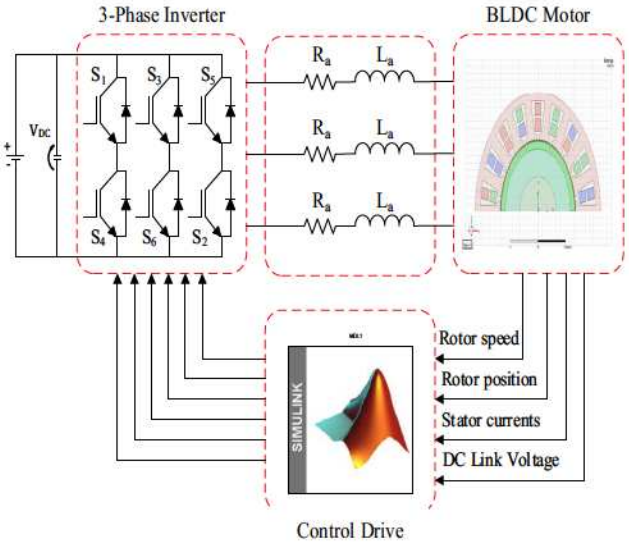

Fig. 2. Co-simulation setup in Ansys Twin Builder.

TABLE II. ESD VALUES FOR OPEN-CIRCUIT SWITCH FAULT

Switch		**S_1**	
Phase	A	B	C
ESD before fault	6191	6126	6283
ESD after fault	2296	5374	5309
ESD error	-3895	-751	-974
Switch		**S_4**	
Phase	A	B	C
ESD before fault	6203	6276	6285
ESD after fault	3625	7256	6768
ESD error	-2577	980	482

For example, the maximum ESD error corresponds to phase B and phase C when the open-circuit fault occurs in S_3 and S_5, respectively. Based on the obtained ESD error, the proposed method can not only detect the fault but also identify the faulty switch. Fault flags, e.g., faulty switch flag (FSF) and faulty phase flag (FPF), are used for fault identification and detection. Fault flags of the inverter switches are determined according to the values of the ESD errors, as revealed in Table III. For example, the maximum ESD error corresponds to the faulty phase, i.e., FPF is '1', '2', and '3' when phases a, b, and c are faulty, respectively. Moreover, the sign of the FSF is determined with respect to the sign of the ESD error, e.g., the FSF is '1' when the ESD error is positive. It can be noted that the fault flags of the switches S_1 and S_4 in Table III are adjusted on the ESD errors in Table II.

Fig. 3 shows the structure of the proposed fault diagnosis methodology. First, the reference current, i*, is adjusted based on the error of reference and measured speeds using a proportional integral (PI) controller. Then, the phase currents are continuously measured during the BLDC motor operation and the rotor position is determined using Hall Effect sensors.

TABLE III. FAULT FLAGS OF THE INVERTER SWITCHES

	FSF phase A	FSF phase B	FSF phase C	FPF
S_1	-1	-1	-1	1
S_4	-1	1	1	1
S_3	-1	-1	-1	2
S_6	1	-1	1	2
S_5	-1	-1	-1	3
S_2	1	1	-1	3

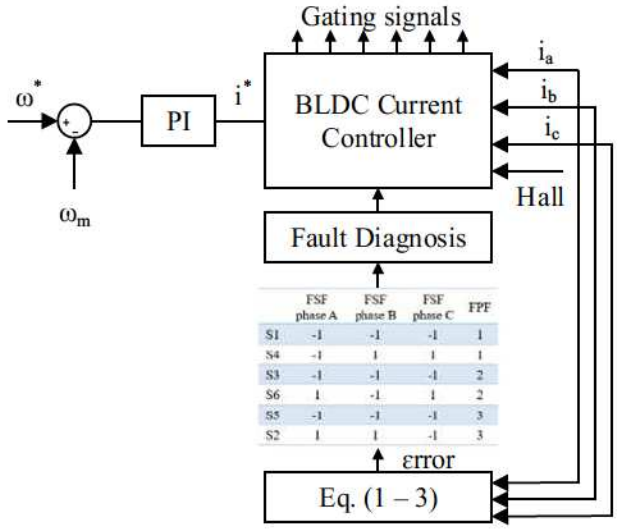

Fig. 3. Structure of the proposed fault diagnosis.

After that, the DFT and ESD are calculated by Eq. (1) and Eq. (2), respectively. The ESD error, computed by Eq. (3), is measured by comparing the ESD values of the current and previous time intervals. Accordingly, a knowledge-based table is developed for fault diagnosis and identification under possible fault scenarios, as revealed in Table III. Finally, high-frequency gating signals are applied to the six switches of the employed inverter. It is worth mentioning that the minimum time interval for accurate fault detection is one electrical cycle.

III. CO-SIMULATION RESULTS

This section presents the co-simulation results of the BLDC motor dive using the Ansys Twin Builder under healthy and open-circuit fault scenarios. Simulation results have been carried out in the cases of open-circuit faults of the six inverter switches. As an illustrative example, one case is presented when the open-circuit fault of the upper switch S_1 is applied at $t = 1$ sec. It is clear that the rotor measured speed follows the reference speed in both healthy and faulty cases, as shown in Fig. 4(a). However, speed oscillations considerably increase during the S_1 open-circuit fault. Moreover, the three-phase stator currents and their associated frequency spectrum are shown in Figs. 5(a) and 6(a), respectively. Under BLDC motor healthy operation, the stator currents are balanced, as shown in Fig. 5(a). However, the

current of phase A becomes significantly distorted, i.e., the current is flowing only during the negative half cycle, and the currents of phases B and C have been changed, i.e., the currents do not flow through motor windings based on the rotor position, during the S_1 open-circuit fault. Furthermore, the frequency spectrum of the stator currents is depicted in Fig. 6(a), showing that the three phases have the same frequency spectrum with only odd harmonics under the healthy case. Whereas, the frequency spectrum is totally changed according to the changes in the phase currents' patterns under the faulty case, and both odd and even harmonics exist. In that case, phase A has the maximum ESD error.

Another case is introduced when the open-circuit fault of the lower switch S_4 is presented at $t = 1$ sec. These two cases are investigated to show the BLDC motor performance when phase A fails, and similar results can be obtained when the remaining two phases fail owing to the symmetry of the employed motor. Fig. 4(b) presents both the reference and measured speeds under healthy and faulty cases, highlighting that the measured speed tracks the reference one with significant oscillations when the S_4 fault is applied. Unlike the first case under the S_1 open-circuit fault, the current of phase A is flowing only during the positive half cycle when the open-circuit fault of S_4 is introduced, as shown in Fig. 5(b). Similarly, the three-phase currents are balanced under healthy conditions, and phase B and phase C currents are affected under faulty conditions. The frequency spectrum of the three-phase stator currents is depicted in Fig. 6(b) in both healthy and faulty cases. Under healthy conditions, the frequency spectrum is the same for the three phases with only odd harmonics. On the contrary, even harmonics exist under faulty conditions due to the changes in the current waveform. Again, the maximum ESD error corresponds to phase A.

Furthermore, the robustness of the proposed inverter fault detection method has been proved under various load and speed scenarios, as listed in Table IV. Numerous cases have been introduced at the rated speed while changing the load. For each case, not only the ability to diagnose the fault is examined but also the capability to identify the faulty switch is checked as well. For each case, the fault is generated at the six inverter switches, and the ESD errors are calculated, as explained in the previous section. The validity of the proposed diagnosis technique is classified based on the fault diagnosis and identification capabilities, e.g., cases 1 and 4 are valid for fault detection and localization. However, some cases are only valid for fault diagnosis and are not capable of fault identification, such as cases 3 and 5. The main drawback of the proposed diagnosis technique is that it fails at low speeds, as proved by case 6. Intensive work will be done to improve the robustness of the proposed technique under low-speed conditions.

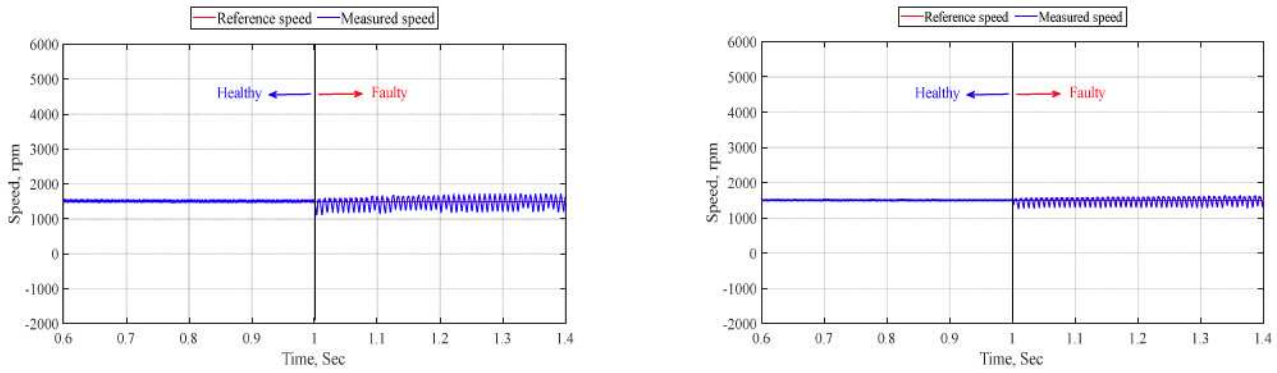

Figure 4: Rotor speed of the BLDC motor under inverter switches faults. (a) switch S_1. (a) switch S_4.

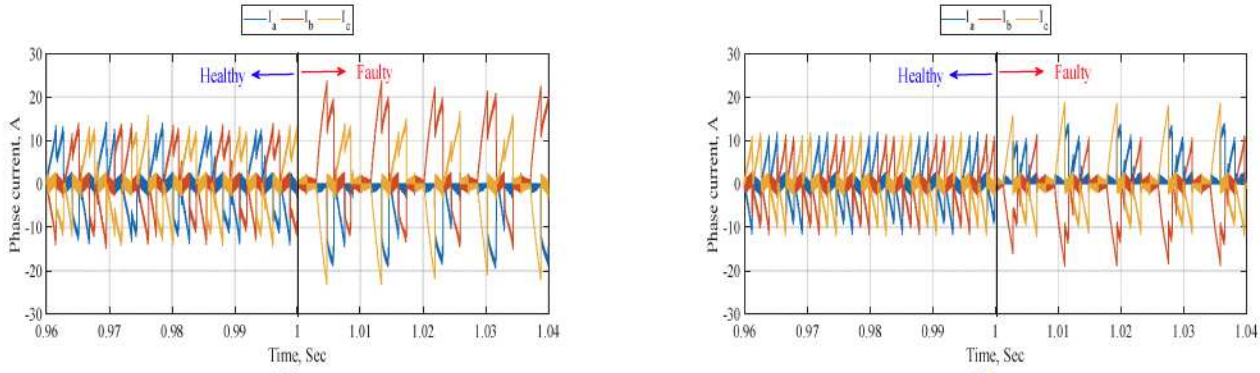

Figure 5: Stator currents of the BLDC motor under inverter switches faults. (a) switch S_1. (a) switch S_4.

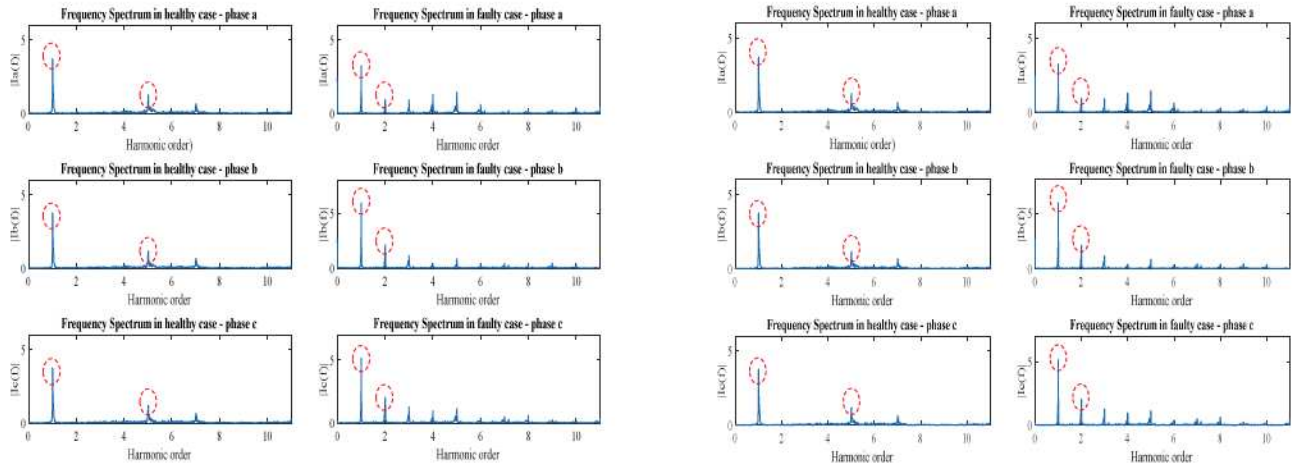

Figure 6: Frequency spectrum of stator currents under inverter switches faults. (a) switch S_1. (a) switch S_4.

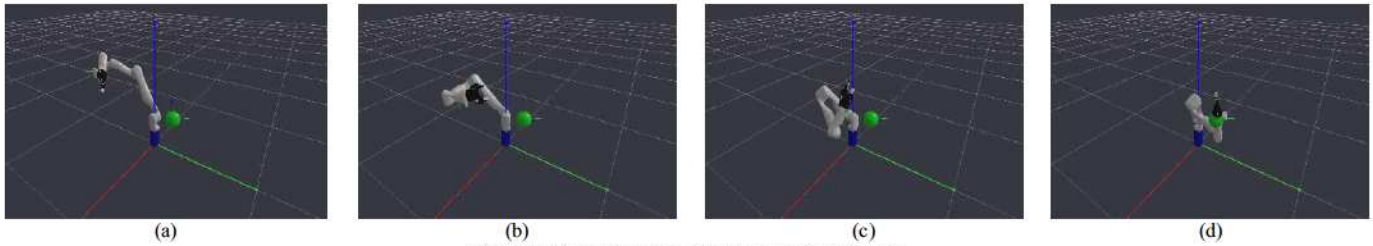

Figure 7: Kinova Gen3 robotic arm under health case.

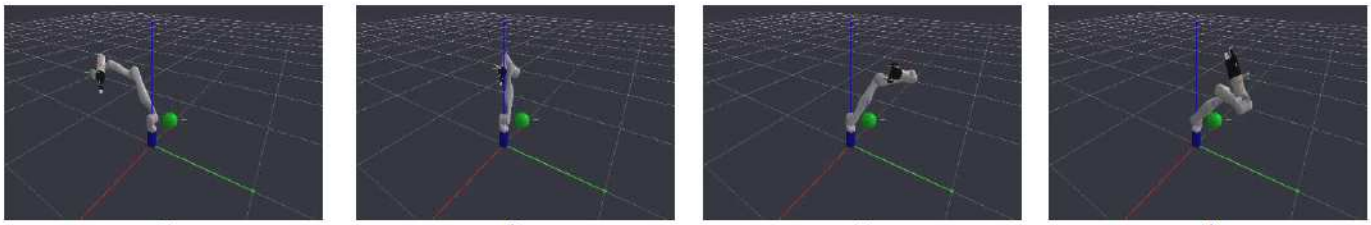

Figure 8: Kinova Gen3 robotic arm under faulty case.

TABLE IV. ROBUSTNESS ANALYSIS

Case	Speed (rpm)	Torque (pu)	Validity
1	1500	0.25	✓
2	1500	0.5	✓ Except S_1 and S_4
3	1500	0.75	✓ Only for phases
4	1500	1	✓
5	1000	1	✓ Only for phases
6	500	1	×

To further highlight the efficacy of the inverter open-circuit fault diagnosis for robot joint motors, the PyBullet software has been utilized to run simulations on the Kinova Gen3 robot arm under healthy and faulty cases, as shown in Figs. 7 and 8, respectively. Fig. 7 shows that the robot can reach its desired end-effector location, highlighted as a green point when no joint failures occur. On the contrary, the same desired workspace location cannot be reached when locked-joint failures happen, as shown in Fig. 8.

IV. CONCLUSION

In this paper, a robust inverter fault diagnosis technique is proposed for BLDC motor drive systems based on the measured phase current information. FEA-based co-simulations are carried out to verify the proposed methodology when an open-circuit fault of the switch occurs. This paper considers the effect of the inverter switch faults not only on the motor level but also on the robotic system level. Validation on the Kinova Gen3 robotic arm has been added to further show the efficacy of the proposed fault diagnosis methodology. Finally, the robustness of the proposed fault diagnosis technique has been tested under various load and speed conditions.

Based on the analysis of fault types presented in this study, fault prognostics and diagnostics in electric motor drives are of particular interest due to both improving the system's reliability and avoiding potential economic loss. For future work, a motor-

drive prototype will be implemented to verify the proposed inverter fault detection approach.

REFERENCES

[1] Z. Mu, L. Han, W. Xu, B. Li, and B. Liang, "Kinematic analysis and fault-tolerant trajectory planning of space manipulator under a single joint failure," Robotics and biomimetics, vol. 3, no. 1, pp. 1-10, 2016.

[2] M. U. Farooq, A. Eizad, and H.-K. Bae, "Power solutions for autonomous mobile robots: A survey," Robotics and Autonomous Systems, vol. 159, p. 104285, 2023.

[3] M. E. Moran, "Evolution of robotic arms," Journal of robotic surgery, vol. 1, no. 2, pp. 103-111, 2007.

[4] T. B. Sheridan, "Human–robot interaction: status and challenges," Human factors, vol. 58, no. 4, pp. 525-532, 2016.

[5] D. Zhu, Y. Ma, M. Wang, J. Yang, Y. Yin, and S. Liu, "LSO-FastSLAM: A New Algorithm to Improve the Accuracy of Localization and Mapping for Rescue Robots," Sensors, vol. 22, no. 3, p. 1297, 2022.

[6] W. Wang, W. Gao, S. Zhao, W. Cao, and Z. Du, "Robot protection in the hazardous environments," in Robots Operating in Hazardous Environments: IntechOpen, 2017, pp. 87-107.

[7] T. Stolte et al., "Taxonomy to Unify Fault Tolerance Regimes for Automotive Systems: Defining Fail-Operational, Fail-Degraded, and Fail-Safe," IEEE Transactions on Intelligent Vehicles, vol. 7, no. 2, pp. 251-262, 2021.

[8] S. B. Niku, Introduction to robotics: analysis, systems, applications. Prentice hall New Jersey, 2001.

[9] M. Quigley, A. Asbeck, and A. Ng, "A low-cost compliant 7-DOF robotic manipulator," in 2011 IEEE International Conference on Robotics and Automation, 2011: IEEE, pp. 6051-6058.

[10] A. Zhao, "Design of a brushless servomotor for a low-cost compliant robotic manipulator," Master's thesis, EECS Department, University of California, Berkeley, 2018.

[11] C. Hwang, P. L. Li, C.-T. Liu, and C. Chen, "Design and analysis of a brushless DC motor for applications in robotics," IET electric power applications, vol. 6, no. 7, pp. 385-389, 2012.

[12] B. Xie and A. A. Maciejewski, "Maximizing the probability of task completion for redundant robots experiencing locked joint failures," IEEE Transactions on Robotics, vol. 38, no. 1, pp. 616-625, 2021.

[13] Y. Da, X. Shi, and M. Krishnamurthy, "Health monitoring, fault diagnosis and failure prognosis techniques for Brushless Permanent Magnet Machines," in 2011 IEEE Vehicle Power and Propulsion Conference, 2011: IEEE, pp. 1-7.

[14] Z. Yin, N. Hu, J. Chen, Y. Yang, and G. Shen, "A review of fault diagnosis, prognosis and health management for aircraft electromechanical actuators," IET Electric Power Applications, vol. 16, no. 11, pp. 1249-1272, 2022.

[15] X. Li, S. Li, W. Chen, T. Shi, and C. Xia, "A Fast Diagnosis Strategy for Inverter Open-circuit Faults Based on the Current Path of Brushless DC Motors," IEEE Transactions on Power Electronics, 2023.

[16] A. Tashakori and M. Ektesabi, "Inverter Switch Fault Diagnosis System for BLDC Motor Drives," Engineering Letters, vol. 22, no. 3, 2014.

[17] J. Fang, W. Li, H. Li, and X. Xu, "Online inverter fault diagnosis of buck-converter BLDC motor combinations," IEEE Transactions on Power Electronics, vol. 30, no. 5, pp. 2674-2688, 2015.

[18] W. Huang et al., "Open-circuit fault detection in PMSM drives using model predictive control and cost function error," IEEE Transactions on Transportation Electrification, vol. 8, no. 2, pp. 2667-2675, 2021.

[19] B.-G. Park, K.-J. Lee, R.-Y. Kim, T.-S. Kim, J.-S. Ryu, and D.-S. Hyun, "Simple fault diagnosis based on operating characteristic of brushless direct-current motor drives," IEEE Transactions on Industrial Electronics, vol. 58, no. 5, pp. 1586-1593, 2011.

[20] W. Huang et al., "Current-based open-circuit fault diagnosis for PMSM drives with model predictive control," IEEE Transactions on Power Electronics, vol. 36, no. 9, pp. 10695-10704, 2021.

[21] H. Yan, Y. Xu, F. Cai, H. Zhang, W. Zhao, and C. Gerada, "PWM-VSI fault diagnosis for a PMSM drive based on the fuzzy logic approach," IEEE Transactions on Power Electronics, vol. 34, no. 1, pp. 759-768, 2018.